Optimized Convolutional Neural Network Towards Effective Wafer Defects Classification

Koon Hian Ang[1], Koon Meng Ang[1], Chin Hong Wong[2,3], Abhishek Sharma[4], Chun Kit Ang[1], Kim Soon Chong[1], Sew Sun Tiang[1*], Wei Hong Lim[1*]

[1]*Faculty of Engineering, Technology and Built Environment, UCSI University, Kuala Lumpur 56000, Malaysia*
[2]*Maynooth International Engineering College, Maynooth University, Maynooth, Co Kildare, Ireland*
[3]*Maynooth International Engineering College, Fuzhou University, Fujian, 350116, China*
[4]*Department of Computer Science and Engineering, Graphic Era Deemed to be University, Dehradun 248002, India*
Email: 1001850063@ucsiuniversity.edu.my, 1001436889@ucsiuniversity.edu.my, chinhong.wong@mu.ie, abhishek15491@gmail.com, angck@ucsiuniversity.edu.my, ChongKS@ucsiuniversity.edu.my, tiangss@ucsiuniversity.edu.my, limwh@ucsiuniversity.edu.my

Abstract

Semiconductor defect inspection is crucial for yield improvement but is hindered by manual inspection's subjectivity and error. This paper employs Convolutional Neural Networks (CNNs) for automated wafer defect classification, addressing the challenges of time-intensive training and complex hyperparameter tuning. We propose the Arithmetic Optimization Algorithm (AOA) to efficiently optimize CNN hyperparameters like momentum, initial learning rate, maximum epochs, and L2 regularization. Our method reduces the trial-and-error in hyperparameter tuning. Using the AOA-optimized ResNet-18 model, our simulations show superior performance in defect classification compared to the unoptimized model, demonstrating its effectiveness and practical potential.

Keywords: Arithmetic optimization algorithm, Convolutional neural networks, Hyperparameter optimization, Wafer defect classification

1. Introduction

The advent of the fourth industrial revolution (IR4.0) has escalated the need for semiconductor industries to produce increasingly complex integrated circuit chips. This complexity arises from the need to pattern and etch more components on semiconductor wafers, catering to diverse chip specifications like lifespan, size, memory storage, and access speed. Consequently, this escalation in production demands heightens the likelihood of process-induced defects on wafer surfaces, adversely affecting the manufacturing yield. A key step in mitigating this yield reduction involves the identification and classification of wafer defect patterns, which often correlate with various manufacturing stages, including contamination, robot handoff, and flow leakages. Accurate identification of these defects enables engineers to pinpoint and rectify the underlying issues, thereby enhancing chip production yield [1].

Most semiconductor industries currently depend on manual visual inspection for detecting wafer defects, a method plagued by subjectivity and a high risk of erroneous classifications due to long-term fatigue. To address these limitations, there is a growing need for an automated machine vision system, integrated with an optimized deep learning model, for reliable wafer defect classification. Convolutional Neural Networks (CNNs) are a widely used deep learning technique [2], [3], [4], [5], [6], [7]. particularly effective in wafer defect classification [8], [9], owing to their capability to learn the nonlinearity between inputs and outputs by automatically extracting relevant information from raw data. Pre-trained CNN architectures like GoogleNet [10]. AlexNet [11], VGG [12], and ResNet [13] have been successfully adapted using transfer learning to tackle new tasks, benefiting from reduced data and training time requirements. The efficacy of these pre-trained networks in addressing new tasks through transfer learning process is heavily influenced by the hyperparameter settings employed during their training phase.

In conventional practice, the fine-tuning of CNN hyperparameters relies on a labor-intensive and time-consuming trial-and-error approach. To streamline this process, metaheuristic search algorithms (MSAs), drawing inspiration from various natural phenomena [14]—including swarm intelligence, natural evolution, physics, mathematical principles, and human activities—have been developed. These algorithms are effective in addressing complex problems [15], [16], [17], [18], [19], [20], [21], [22] and are particularly adept at hyperparameter tuning in CNNs [23], thanks to their robust global search capabilities. One such algorithm is the Arithmetic Optimization Algorithm (AOA) [24], which derives its strategy from the distribution behaviors of basic arithmetic operations such as addition, subtraction, multiplication, and division.

In this study, we employ a pre-trained network, ResNet-18, retrained on new datasets using transfer learning for

the purpose of wafer defect classification. The AOA is utilized to optimize four critical hyperparameters of the CNN: momentum, initial learning rate, maximum epochs, and L2 regularization. The efficacy of this optimized CNN model in classifying wafer defects is then assessed and benchmarked against the performance of a corresponding unoptimized CNN model.

2. Related Works

2.1. *Conventional CNN and ResNet-18*

A typical CNN architecture comprises three fundamental components: convolutional layers (Conv) for feature extraction, pooling (Pool) layers for reducing the size of feature maps, and fully connected (FC) layers for classification. Table 1 illustrates an example of a standard CNN model.

Table 1. Architecture of a typical CNN.

Layer	Layer Type	#Feature Maps	Feature Map Size	Filter Size
1	Input	1	14×14	
2	Conv 1	6	7 × 7	5×5
3	Pool 1	6	4×4	2 ×2
4	Conv 2	16	4×4	5 × 5
5	Pool 2	16	2 × 2	2 × 2
6	FC 1	1	120	
7	FC 2	1	84	

He et al. [13] introduced ResNet models, known for their deep architectures, which have exhibited remarkable convergence and high accuracy. In 2015, ResNet models achieved first place in the ImageNet Large Scale Visual Recognition Challenge (ILSVRC) and the Common Objects in Context (COCO) classification challenge. ResNet is characterized by multiple stacked residual units and comes in various configurations, including 18, 34, 50, 101, 152, and 1202 layers, each with specific operations tailored to its architecture. ResNet-18, a model offering an optimal balance between depth and performance, comprises five convolutional layers, one average pooling layer, and a fully connected layer with SoftMax activation. ResNet-50 includes 49 convolutional layers, culminating in a fully connected layer. Considering the balance between computational efficiency and performance, ResNet-18 is chosen for this study.

2.2. *Arithmetic optimization algorithm (AOA)*

In 2021, Abualigah et al. [24] introduced the AOA, a MSA inspired by the characteristics of the four basic arithmetic operations: addition, subtraction, multiplication, and division. The AOA operates through three primary phases: initialization, exploration, and exploitation, strategically navigating the solution space to address optimization challenges effectively.

In the initialization phase of the AOA, a set of potential solutions is generated, each falling within predefined dimensional boundaries, to address specific optimization problems. Subsequently, the algorithm calculates the Math Optimizer Accelerated (MOA) value, which dictates the search strategy between exploration and exploitation phases. The MOA function is mathematically expressed as:

$$MOA(C_{Iter}) = Min + C_{Iter} \times \left(\frac{Max - Min}{M_{Iter}}\right) \quad (1)$$

where $\boldsymbol{C_{Iter}}$denotes the current iteration number, $\boldsymbol{M_{Iter}}$ is the maximum number of iterations, and *Min* and *Max* are the lower and upper limits of the accelerated function, respectively. The AOA enters the exploration phase if the MOA value is lower than a randomly generated number between 0 and 1; otherwise, it proceeds to the exploitation phase.

During the exploration phase of the AOA, both Multiplication and Division operators are employed to enhance the search space coverage and introduce a diverse array of solutions. This approach leverages their potential for high dispersion and distributed values. The position of each *i*-th AOA solution in the *d*-th dimension is updated as follows:

$$x_{i,j}(C_{Iter}+1) = \begin{cases} x_j^{best} \div (MOP+\varepsilon) \times \left(\left(UB_j - LB_j\right) \times \mu + LB_j\right), & r1 < 0.5 \\ x_j^{best} \times MOP \times \left(\left(UB_j - LB_j\right) \times \mu + LB_j\right), & \text{otherwise} \end{cases} \quad (2)$$

where $x_{i,j}(C_{Iter}+1)$ denotes the *j*-th dimension of the *i*-th solution in the next iteration $(C_{Iter}+1)$, with *j* ranging from 1 to *D*, *i* ranging from *1* to *I*, and *I* is the population size; C_{Iter} ranges from 1 to M_{Iter}, the latter is the algorithm's maximum iteration number; x_j^{best} is the *j*-th dimension of the best solution; UB_j and LB_j are the upper and lower boundaries in the *j*-th dimension; $r1$ is a random number between 0 and 1; μ adjusts the search range. Define the Math Optimizer Probability (MOP) as:

$$MOP(C_{Iter}) = 1 - \frac{C_{Iter}^{\frac{1}{\alpha}}}{M_{Iter}^{\frac{1}{\alpha}}} \quad (3)$$

where $MOP(C_{Iter})$ represents the function value at iteration C_{Iter}, and α controls the exploitation accuracy.

In the exploitation phase of the AOA, Subtraction and Addition operators are utilized to precisely target the search regions identified by the most promising AOA solution. This step leverages the operator's characteristic of being densely concentrated yet having low dispersion. The position of each *i*-th AOA solution in the *d*-th dimension is updated as follows during this phase:

$$x_{i,j}(C_{Iter}+1) = \begin{cases} x_j^{best} - MOP \times \left((UB_j - LB_j) \times \mu + LB_j \right), & r2 < 0.5 \\ x_j^{best} + MOP \times \left((UB_j - LB_j) \times \mu + LB_j \right), & \text{otherwise} \end{cases} \quad (4)$$

Here, $\boldsymbol{r2}$ represents a randomly generated number between 0 and 1, following a uniform distribution.

The AOA algorithm iteratively executes these exploration and exploitation processes until predefined stopping criteria are met. The optimal solution generated by AOA at the end of the optimization process is adopted as the best set of hyperparameters for training the ResNet-18 network to classify wafer defects**.**

3. Proposed Optimized Deep Learning Model

3.1. *Preprocessing of dataset with wafer defects*

The optimized ResNet-18 architecture undergoes training and evaluation for wafer defect classification utilizing the WM-811K dataset [25]. This particular dataset is noted for its significantly imbalanced distribution across various classes. To mitigate potential biases and overfitting stemming from this imbalance, we formed a new dataset using an under-sampling method. This approach involved compiling 30,000 images classified as 'None defect' from the WM-811K dataset, along with all other images categorized as defects. The resultant dataset, balanced in terms of defect and non-defect images, is detailed in Table 2, providing a comprehensive breakdown of the image categories.

Table 2. Number of defect and non-defect wafer images after preprocessing stage

Layer	Defect Type	#Labeled Images
1	Center	4,294
2	Donut	555
3	Edge-Loc	5,189
4	Edge-Ring	9,680
5	Loc	3,593
6	Near-Full	149
7	Random	866
8	Scratch	1,193
9	None	30,000

3.2. *Hyperparameter tuning of ResNet-18 with AOA*

The revised WM-811K dataset, detailed in Table 2, is used to train the chosen deep learning model, ResNet-18, for wafer defect classification via transfer learning. To tailor the pre-trained network for this specific classification task, several modifications are made to both the input datasets and the configuration of ResNet-18. The size of each input image is increased from 48×48×1 to 224×224×3, the padding size of the initial convolution layer is adjusted to align with the new input size, and the output size of the fully connected layer is altered to 9 to reflect the nine defect types identified in this study.

Additionally, to enhance ResNet-18's performance in classifying wafer defects, the AOA is implemented to optimize the network's training hyperparameters during the transfer learning process. The AOA generates solution vectors representing four key decision variables: momentum, initial learning rate, maximum epochs, and L2 regularization. The ranges for these variables are specified in Table 3. The effectiveness of each AOA solution is assessed based on the classification accuracy achieved. Fig. 1 illustrates the AOA-optimized ResNet-18 framework developed for wafer defect classification.

Table 3. Lower and upper bounds of training hyperparameters to be optimized.

Hyperparameter	Lower Limits	Upper Limits
Momentum	0.5	0.9
Initial Learning Rate	0.01	0.1
Maximum Epochs	5	10
L2 Regularization	1×10^{-4}	5×10^{-4}

AOA-Optimized ResNet-18 for Wafer Defect Classification

Input: *N*, *D*, UB_j, LB_j
Initialize $C_{Iter} = 0$;
for *i* =1 to *I* **do**
  Randomly generate solution x_i;
  $C_{Iter} = C_{Iter} + 1$;
end for
while $C_{Iter} \leq M_{Iter}$ **do**
  Decode the hyperparameters from x_i;
  Train the ResNet-18 using transfer learning based on hyperparameters decoded from x_i;
  Evaluate the accuracy $f(x_i)$ of ResNet-18;
  Calculate *MOP* using Eq. (3);
  Calculate *MOA* using Eq. (1);
  for *i* =1 to *I* **do**
    for *j* =1 to *D* **do**
      if *rand* > *MOA* **then**
        Update $x_{i,j}(C_{Iter}+1)$ with Eq. (2);
      Else
        Update $x_{i,j}(C_{Iter}+1)$ with Eq. (4)
      end if
    end for
    Decode the hyperparameters from x_i;
    Train the ResNet-18 using transfer learning based on hyperparameters decoded from x_i;
    Evaluate the accuracy $f(x_i)$ of ResNet-18;
    Update x_i, $f(x_i)$, x^{best}, $f(x^{best})$
    $C_{Iter} \leftarrow C_{Iter} + 1$;
  end for
end while

Output: Optimal values of momentum, initial learning rate, maximum epochs and L2 regularization decoded from the best AOA solution represented as x^{best}.

Fig.1 Pseudocode of optimizing the hyperparameters of ResNet-18 using AOA for wafer defect classification.

4. Performance Studies

4.1. *Simulation settings*

The pre-processed WM-811K dataset is randomly partitioned into three subsets for the purposes of training, validation, and testing. Specifically, the dataset allocation

comprises 70% for training, 10% for validation, and 20% for testing. Additionally, all input images are uniformly resized to a dimension of 224×224×3, and the minimum batch size for processing is set as 32.

4.2. *Performance comparisons*

The classification effectiveness of both unoptimized ResNet-18 and AOA-Optimized ResNet-18 in identifying wafer defects is evaluated using several key metrics: recall, accuracy, precision, F1 score, and AUC. Consider *TP*, *TN*, *FP*, and *FN* as the true positive, true negative, false positive, and false negative counts, respectively, generated by the deep learning model during the classification process. Recall, reflecting the model's capability to detect positive samples, is calculated as:

$$Recall = \frac{TP}{TP + FN} \tag{5}$$

Accuracy, indicating the proportion of correctly predicted data, is defined as:

$$Accuracy = \frac{TP + TN}{TP + TN + FP + FN} \tag{6}$$

Precision, measuring the model's accuracy in predicting a sample as positive, is expressed as:

$$Precision = \frac{TP}{TP + FP} \tag{7}$$

The F1 score, the harmonic mean of precision and recall, is calculated by:

$$F1\ Score = 2 \times \left(\frac{Precision \times Recall}{Precision + Recall}\right) \tag{8}$$

Lastly, AUC, representing the area under the receiver operating characteristic curve, provides an overall effectiveness measure. The quantitative performance of both the unoptimized and AOA-Optimized ResNet-18 models is detailed in Table 4. Additionally, their qualitative performance is analyzed based on the confusion matrices depicted in Fig. 2.

Table 4. Quantitative performance comparison between optimized and unoptimized ResNet-18

Metrics	Unoptimized ResNet-18	AOA-Optimized ResNet-18
Validation Accuracy	0.8560	**0.8983**
Testing Accuracy	0.8388	**0.8923**
Recall	0.8482	**0.8956**
Precision	0.8751	**0.9059**
F1 Score	0.8523	**0.8972**
AUC	0.9002	**0.9397**

Table 4 illustrates that the AOA-optimized ResNet-18 surpasses the unoptimized model in all assessed metrics. It shows a higher validation accuracy of 0.8983 compared to the unoptimized model's 0.8560, and a testing accuracy of 0.8923 versus 0.8388. Additionally, the recall score of the AOA-optimized model stands at 0.8956, outperforming the unoptimized model's 0.8420. In terms of precision, the AOA-optimized model achieves a score of 0.9059, exceeding the unoptimized model's 0.8751. The F1 score and AUC for the optimized model are 0.8972 and 0.9397, respectively, both higher than the unoptimized model's scores of 0.8523 and 0.9002. The enhanced validation accuracy of the AOA-optimized ResNet-18 indicates its superior performance in predicting classes of unseen samples during training, while its greater testing accuracy suggests a more accurate prediction of new, unseen data classes. The improved recall and precision scores signify the model's heightened ability to correctly identify more true positive samples and effectively reduce false positives.

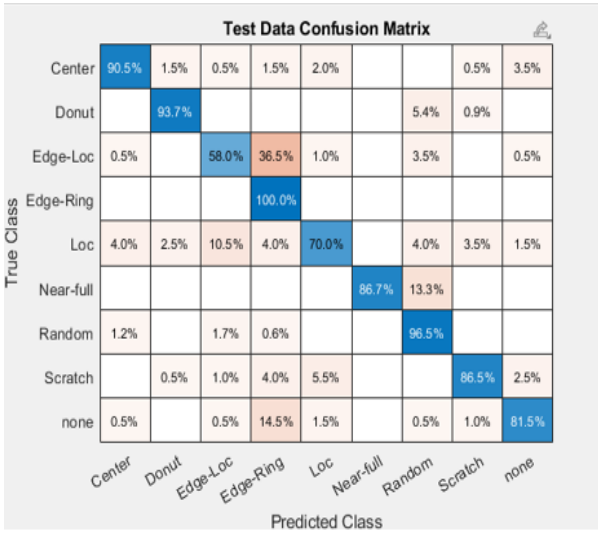

(a)

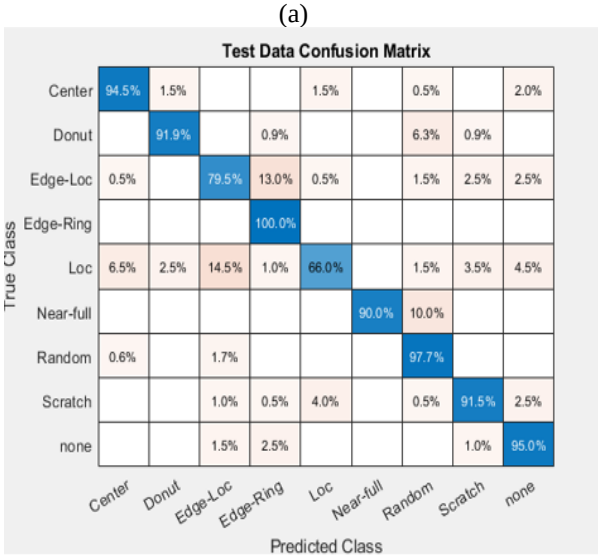

(b)

Fig.2 Confusion matrices produced by: (a) Unoptimized ResNet-18 and (b) AOA-Optimized ResNet-18 when classfying wafer defects.

Qualitative results, derived from confusion matrices of both the AOA-optimized and unoptimized ResNet-18 models as depicted in Fig. 2, align with the quantitative findings in Table 4. The AOA-optimized model demonstrates superior accuracy in classifying various

wafer defects, including Center, Edge-Loc, Near-Full, Random, and Scratch, compared to the unoptimized version. Notably, the unoptimized model frequently misclassifies Edge-Loc defects as Edge-Ring, leading to significant errors, and incorrectly labels 14.5% of 'No defect' cases as Edge-Ring defects. Both the quantitative and qualitative analyses suggest that optimizing ResNet-18's hyperparameters through AOA effectively corrects the misclassification issues observed in the unoptimized model, resulting in a marked enhancement in the model's ability to classify wafer defects accurately and efficiently.

5. Conclusion

This study is designed to demonstrate the effectiveness of optimizing hyperparameters in deep learning models for wafer defect classification. In our approach, the Arithmetic Optimization Algorithm (AOA) is employed to fine-tune four key hyperparameters—momentum, initial learning rate, maximum epoch, and L2 regularization rate—of the ResNet-18 model. This model, initially pre-trained on ImageNet, was further refined on a wafer defect dataset via transfer learning. Our extensive simulation studies indicate that the AOA-optimized ResNet-18 model surpasses the unoptimized version in recall, accuracy, precision, F1 score, and AUC, showcasing enhanced capabilities in accurately identifying and classifying wafer defects.

The findings reveal the significance of hyperparameter optimization in developing deep learning models for wafer defect classification. Future research could investigate the applicability of AOA in fine-tuning other deep learning models within this domain. Additionally, exploring AOA for identifying optimal deep learning network architectures offers promising avenues for robust wafer defect classification. Incorporating more features and diverse data sources could further refine the proposed method's efficacy. Finally, subsequent studies should assess the practicality of implementing these optimized deep learning models in industrial settings for real-world wafer defect classification applications.

Acknowledgements

This work was supported by UCSI University's Research Excellence & Innovation Grant (REIG) with project code of REIG-FETBE-2022/038 and Billion Prima Sdn. Bhd.'s Industry Research Grant with project code of IND-FETBE-2023/006.

References

1. J. C. Chien, M. T. Wu and J. D. Lee, Inspection and classification of semiconductor wafer surface defects using CNN deep learning networks, Applied Sciences 10(15), 2020, pp. 5340.
2. B. Jdid, W. H. Lim, I. Dayoub, K. Hassan and M. R. B. M. Juhari, Robust automatic modulation recognition through joint contribution of hand-crafted and contextual features, IEEE Access 9, 2021, pp. 104530-104546.
3. M. Alrifaey et al., Hybrid deep learning model for fault detection and classification of grid-connected photovoltaic system, IEEE Access 10, 2022, pp. 13852-13869.
4. T. Berghout, L. H. Mouss, T. Bentrcia and M. Benbouzid, A semi-supervised deep transfer learning approach for rolling-element bearing remaining useful life prediction, IEEE Transactions on Energy Conversion 37(2), 2022, pp. 1200-1210.
5. O. Friha, M. A. Ferrag, M. Benbouzid, T. Berghout, B. Kantarci and K.-K. R. Choo, 2DF-IDS: Decentralized and differentially private federated learning-based intrusion detection system for industrial IoT, Computers & Security 127, 2023, pp. 103097.
6. T. Berghout, M. Benbouzid, Y. Amirat and G. Yao, Lithium-ion battery state of health prediction with a robust collaborative augmented hidden layer feedforward meural network approach, IEEE Transactions on Transportation Electrification 9(3), 2023, pp. 4492-4502.
7. L. S. Chow, G. S. Tang, M. I. Solihin, N. M. Gowdh, N. Ramli and K. Rahmat, Quantitative and qualitative analysis of 18 deep convolutional neural network (CNN) models with transfer learning to diagnose COVID-19 on chest X-ray (CXR) images, SN Computer Science 4(2), 2023, pp. 141.
8. U. Batool, M. I. Shapiai, M. Tahir, Z. H. Ismail, N. J. Zakaria and A. Elfakharany, A systematic review of deep learning for silicon wafer defect recognition, IEEE Access 9, 2021, pp. 116572-116593, 2021.
9. S. Chen, Y. Zhang, M. Yi, Y. Shang and P. Yang, AI classification of wafer map defect patterns by using dual-channel convolutional neural network, Engineering Failure Analysis 130, 2021, pp. 105756.
10. C. Szegedy et al., Going Deeper with Convolutions, 2015 IEEE Conference on Computer Vision and Pattern Recognition (CVPR), Boston, MA, USA, 2015, pp. 1-9.
11. A. Krizhevsky, I. Sutskever and G. Hinton, ImageNet classification with deep convolutional neural networks, Neural Information Processing Systems 25, 2012.
12. K. Simonyan and A. Zisserman, Very deep convolutional networks for large-scale image recognition, arXiv 1409.1556, 2014.
13. K. He, X. Zhang, S. Ren and J. Sun, Deep Residual Learning for Image Recognition, 2016 IEEE Conference on Computer Vision and Pattern Recognition (CVPR), Las Vegas, NY, USA, 2016, pp. 770-778.
14. M. F. Ahmad, N. A. M. Isa, W. H. Lim and K. M. Ang, Differential evolution: A recent review based on state-of-the-art works, Alexandria Engineering Journal 61(5), 2022, pp. 3831-3872.
15. M. Shaari et al., Supervised evolutionary programming based technique for multi-DG installation in distribution system, IAES International Journal of Artificial Intelligence 9, 2020, pp. 11.
16. K. M. Ang et al., Modified teaching-learning-based optimization and applications in multi-response machining processes, Computers & Industrial Engineering 174, 2022, pp. 108719.
17. A. Sharma, A. Sharma, V. Jately, M. Averbukh, S. Rajput, and B. Azzopardi, A novel TSA-PSO based hybrid slgorithm for GMPP tracking under partial shading conditions, Energies, 15, 2022, pp. 3164.
18. A. Singh, A. Sharma, S. Rajput, A. K. Mondal, A. Bose and M. Ram, Parameter extraction of solar module using the sooty tern optimization algorithm, Electronics 11, 2022, pp. 564.
19. C. Hassan, V. Durai, S. Sapuan, N. A.A and M. Z. Mohamed Yusoff, Mechanical and crash performance of unidirectional oil palm empty fruit bunch fibre-reinforced polypropylene composite, Bioresources 13, 2018, pp. 8310-8328.

20. E. Natarajan, C. Hassan, C. K. Ang, M. S. Santhosh, S. Ramesh and R. Sasikumar, Modeling of multiwall carbon nanotubes reinforced natrual rubber for soft robotic applications - A comprehessive presentation 46(9), 2021, pp. 3251-3258.
21. A. Machmudah et al. Cyclic path planning of hyper-redundant manipulator using whale optimization algorithm, International Journal of Advanced Computer Science and Applications 12(8), 2021, pp. 677-686.
22. K. Palanikumar, J. Nithyanandam, E. Natarajan, W. H. Lim and S. S. Tiang, Mitigated cutting force and surface roughness in titanium alloy-multiple effective guided chaotic multi objective teaching learning based optimization, Alexandria Engineering Journal 64, 2023, pp. 877-905.
23. K. M. Ang et al., Optimal design of convolutional neural network architectures using teaching and learning-based optimization for image classification, Symmetry 14(11), 2022, pp. 2323.
24. L. Abualigah, A. Diabat, S. Mirjalili, M. Abd Elaziz and A. H. Gandomi, The Arithmetic Optimization Algorithm, Computer Methods in Applied Mechanics and Engineering 376, 2021, pp. 113609.
25. J.-S. R. Jang. MIR-WM811K wafer map, http://mirlab.org/dataSet/public/

Authors Introduction

Mr. Koon Hian Ang

He received the Bachelor of Mechatronics Engineering with Honours in Faculty of Engineering, Technology and Built Environment, UCSI University, Malaysia, in 2023. His research interests are machine learning, deep learning, and optimization algorithm.

Dr. Koon Meng Ang

He received the B.Eng. degree in Mechatronic Engineering with Honours and PhD in Engineering from UCSI University, Malaysia, in 2019 and 2023, respectively. His research interests are swarm intelligence, machine learning and deep learning.

Dr. Chin Hong Wong

He is a Lecturer in Maynooth International Engineering College at Fuzhou University in China. He received his PhD in Electrical and Electronic Engineering from Universiti Sains Malaysia in 2017. His research interests are Energy harvesting and control system.

Dr. Abhishek Sharma

He is a Research Assistant Professor at Graphic Era Deemed to be University in India. He received his PhD from University of Petroluem & Energy Studies in 2022. His research interests are artificial intellgence and power electronics.

Dr. Chun Kit Ang

He is the Dean and Associate Professor in Faculty of Engineering at UCSI University in Malaysia. He received his PhD in Mechanical and Manufacturing Engineering from Universiti Putra Malaysia in 2014. His research interests are artificial intelligence, soft computing, robotics and mechatronics.

Dr. Kim Soon Chong

He is an Assistant Professor in Faculty of Engineering at UCSI University in Malaysia. He received his PhD in Electrical, Eleronics & System Engineering from Universiti Kebangsaan Malaysia in 2022. His research interests are biomedical and healthcare technoologies.

Dr. Sew Sun Tiang

She is an Assistant Professor in Faculty of Engineering at UCSI University in Malaysia. She received her PhD in Electrical and Electronic Engineering from Universiti Sains Malaysia in 2014. Her research interests are optimization and antenna design.

Dr. Wei Hong Lim

He is an Associate Professor in Faculty of Engineering at UCSI University in Malaysia. He received his PhD in Computational Intelligence from Universiti Sains Malaysia in 2014. His research interests are optimization and artificial intelligence.